Environmental Science and Pollution Research (2019) 26:7614–7626
https://doi.org/10.1007/s11356-019-04173-7

RESEARCH ARTICLE

Adsorption studies of 17β-estradiol from aqueous solution using a novel stabilized Fe–Mn binary oxide nanocomposite

Ming-yang Dai [1,2] · Yun-guo Liu [1,2] · Guang-ming Zeng [1,2] · Shao-bo Liu [3] · Qi-meng Ning [1,2]

Received: 7 October 2018 / Accepted: 4 January 2019 / Published online: 21 January 2019

Abstract

The removal of 17β-estradiol (E2) from contaminated water on nanoscale Fe–Mn binary oxide-loaded multiwalled carbon nanotubes (MWCNTs/FMBO) was evaluated in this work. The characterizations of the mesoporous adsorbent were analyzed by using SEM, TEM, VSM, XRD, XPS, and FTIR measurements. The effects of experimental conditions in E2 removal, including stabilizer additional level, adsorption time, initial E2 concentration, solution pH, reaction temperature, and foreign ions, were examined. The maximum monolayer adsorption capacity (q_m) of MWCNTs/FMBO for E2 in the experiment was 47.25 mg/g as verified by the Langmuir sorption isotherm study. The adsorption process was pH-sensitive with an optimum pH of 7.0. On the kinetics study, the adsorption data could be satisfactorily fitted by the pseudo-second-order kinetics. Thermodynamic parameters indicated that the adsorption process was spontaneous and exothermal. In addition, the foreign ions did not show any noticeable inhibition for E2 removal from the water solution except for PO_4^{3-} that was adversely affected for E2 uptake than other anions in a certain concentration. The adsorption capacities of the mesoporous adsorbent remained at 86.16% even after five adsorption–desorption cycles without significant loss of capacity, which demonstrated the stability and reusability for further removal of E2. Moreover, both hydrogen bond and π–π interaction might be the dominating adsorption mechanisms for E2 adsorption onto MWCNTs/FMBO.

Keywords Multiwalled carbon nanotubes · Fe–Mn binary oxides · Nanoparticles · 17β-Estradiol · Adsorption mechanism

Introduction

The concern of the long-term adverse effects of endocrine-disrupting chemicals (EDCs) in the ecosystem has raised over the last decades (Fan et al. 2013; Johnson et al. 2013), because EDCs have been detected in various water sources and have potential damage on ecological systems (Campbell et al. 2006; Khanal et al. 2006). Estrogens are well known as EDCs, which include endogenous hormones like 17β-estradiol (E2) and synthetic estrogens like 17α-ethinylestradiol (EE2) (Xu et al. 2008). E2 is a steroidal hormone and naturally synthesized by wildlife and livestock to promote their growth and reproduction (Xu et al. 2008). In practice, E2 was widely used in various fields such as medical treatment (Fan et al. 2007). Unfortunately, with the increasing discharge of E2, removing the most widely encountered endocrine disruptor molecules from water has become more challenging (Rodgers-Gray et al. 2001). Furthermore, E2, the major form of estrogens in the environment, has high levels of endocrine interference in the EDCs (Nakada et al. 2004), which pose potential threats to the aquatic ecosystems (Qin et al. 2014) and the endocrine/reproductive functions of humans even at low concentrations (Schmitt et al. 2012). Therefore, there is a pressing need for some economically feasible and effectively treatment methods to control E2 pollution.

Various methods such as photo-assisted catalytic degradation (Zhang et al. 2013), bioremediation (Bradley and Writer

Responsible editor: Tito Roberto Cadaval Jr

Electronic supplementary material The online version of this article (https://doi.org/10.1007/s11356-019-04173-7) contains supplementary material, which is available to authorized users.

✉ Yun-guo Liu
liuyunguo_hnu@163.com

[1] College of Environmental Science and Engineering, Hunan University, Changsha 410082, People's Republic of China

[2] Key Laboratory of Environmental Biology and Pollution Control (Hunan University), Ministry of Education, Changsha 410082, People's Republic of China

[3] School of Metallurgy and Environment, Central South University, Changsha 410083, People's Republic of China

2014), and catalytic degradation (Qin et al. 2014) are effective in removing estrogens from water. No doubt, these estrogen treatment technologies have a certain effect for effective removal of E2, but complicated instruments, rigorous operating requirements, and low solubility and high adhesion property of estrogens have limited the application of photodegradation and microbial degradation of estrogens in developing countries (Xu et al. 2008). Adsorption is deemed to be the simple and convenient method because of availability, low cost, and reusability (Awual 2017a; Awual et al. 2015; Taguchi 2016). Recently, some binary metal oxides such as Fe–Mn hydrous oxide (Szlachta et al. 2012), Mn/Al hydrotalcite (Liu et al. 2009), and Fe–Mn binary oxide (FMBO) (Jiang et al. 2017) have been found to have effective adsorption ability for EDCs from aquatic environment because of larger specific surface area, stronger ion exchange capacity, and concurrent redox reaction compared with the single oxides. However, the properties of nanoparticles of Fe–Mn binary oxides that are easily aggregated in solution have limited its adsorption performance and engineering application (Yan et al. 2017). To overcome the inherent problems of FMBO, some polymers have been used as stabilizers in recent studies to prevent agglomeration of nanoparticles (Awual et al. 2016; Huang et al. 2008; Tang et al. 2008).

In fact, a wide variety of carbon-based adsorption materials have been used for stabilizing Fe–Mn binary oxide nanoparticles in recent studies. Yan et al. (2017) developed a stabilized Fe–Mn nanoparticle and the experimental data exhibited that the product had high stability and better adsorption performance. Xie et al. (2015) fabricated stabilized FMBO nanoparticles that provided higher removal efficiency of selenite (> 3 times) than other reported sorbents. Besides, Tang et al. (2016) synthesized original graphene oxide/Fe–Mn binary oxide (GO/Fe–Mn) materials and the results showed that mercury bioavailability was significantly reduced because of more surface active sites and excellent thermal stability of GO/Fe–Mn. Multiwalled carbon nanotubes (MWCNTs), one of the carbon nanotubes, are widely used in various applications such as construction, aerospace, and medical because of remarkable thermal stability and mechanical properties (Lehman et al. 2011; Moradi et al. 2012; Petersen et al. 2011). Recent studies have shown the potential effectiveness of carbon nanotubes for adsorption of aromatic organic compounds (AOCs) in water (Wang et al. 2015; Zhang et al. 2010b). Therefore, immobilization of binary oxides on the surfaces of carbon nanotubes to prepare the highly efficient nano-adsorbents has been a research hot spot (Awual et al. 2016; Huang et al. 2008; Tang et al. 2008).

In this work, a new type of multiwalled carbon nanotubes/Fe–Mn binary oxide (MWCNTs/FMBO) nanocomposite was synthesized to overcome the drawback of FMBO particles. The new nanocomposite exhibited the effectiveness for E2 removal from water. A range of characterization and adsorption experiments was carried out to understand the surface properties and evaluate the adsorption capacity of materials for E2 removal as an efficient and simple-operation adsorbent. Finally, also the investigation on reusability of materials was conducted for potential application.

Experimental section

Materials and reagents

The MWCNTs (purity > 95%, inside diameter 3~5 nm, outer diameter 8~15 nm, length ~ 50 μm, average specific surface area > 140 m^2/g) for this study were produced by Chengdu Organic Chemistry Co., Ltd., Chinese Academy of Sciences. The water for the experiments was ultrapure water (18.25 MΩ/cm). All the chemicals used in the experiment, such as $MnCl_2$, $MgCl_2$, NaOH, HCl, etc., were of analytical grade and produced by Shanghai Chemical Company. E2 ($C_{18}H_{24}O_2$, purity > 98%, molecular weight 228.29) was provided by Sigma-Aldrich Chemical Corporation. The methanol solution was used as the solvent to prepare the stock solution of E2 with a concentration of 2.5 mg/L and then stored in the dark to avoid possible photodegradation.

Synthesis of MWCNTs/FMBO

MWCNTs were washed with ultrapure water before use. The synthesis process of the target product was as follows. Firstly, MWCNTs were added to the solution containing 10 mL (0.075 M) $Fe(NO_3)_3 \cdot 9H_2O$ and 10 mL (0.025 M) $MnCl_2 \cdot 2H_2O$. The pH of the solution was maintained at 10 with sodium hydroxide solution (1 M) and then stirred continuously for 4 h to complete the reaction. The mixture was stored at room temperature and in dark conditions for 12 h. Secondly, the obtained mixture was cleaned with ultrapure water until the solution pH reached 7.0. Finally, the resulting product was oven-dried at 378 K, then screened and stored at room temperature.

Characterization of MWCNTs/FMBO

The surface morphology and structure of the adsorbent were detected by scanning electron microscopy (SEM) (Hitachi S4800, Japan) and transmission electron microscopy (TEM) (Tecnai G2 F20, USA) (Wang et al. 2014). The specific surface area of the product was characterized by nitrogen adsorption–desorption isotherm using an automatic surface area analysis instrument (Quantachrome, USA) (Xu et al. 2012). The crystal phase composition of the material was measured by X-ray diffraction (XRD) (D8 ADVANCE, Germany) (Wu et al. 2014). Magnetic properties were measured by using a vibrating sample magnetometer (VSM)

(PPMS-9, Quantum Design, USA) at 300 K. For the zeta potential measurements, the sample was determined by using a zeta potential instrument (Zetasizer Nano ZS90, Malvern, UK) (Wu et al. 2014). The changes of surface functional groups and elements during the sorption process were explored by Fourier transform infrared spectrum (FTIR) (Nicolet 5700, USA) and X-ray photoelectron spectroscopy (XPS) (Thermo ESCALAB 250XI, USA) (Wu et al. 2014).

Batch tests for adsorption of E2

The adsorption processes were carried out in glass conical flasks, which contained 100 mL E2 solution and 5 mg MWCNTs/FMBO. The conical flasks were placed in a thermostatic oscillator with an oscillating speed of 160 rotations per minute (rpm) and a temperature of 298 K. After 12 h of reaction, the solution was left to rest for 10 min, then 10 mL of supernatant was extracted and filtered with 0.45 μm membrane filter (Wang et al. 2014; Xu et al. 2012).

The concentration of E2 in solution was determined by using a fluorescence spectrophotometer (Hitachi F-4500, Japan) at 310 nm (Jiang et al. 2016) with an excitation source of 450 W xenon lamp. The equation for calculating the amount of adsorbed E2 is as follows:

$$q_e = \frac{(C_0 - C_e)V}{m} \quad (1)$$

where C_0 is the initial concentration of E2 (mg/L), and C_e is the equilibrium concentration of E2 (mg/L). All C_e values are obtained in the sorption spectrum at 310 nm. V is the solution volume (L) and m is the mass of adsorbent (g).

In order to determine the appropriate amount of stabilizer for synthetic materials, key tests were conducted. The multiwalled carbon nanotubes of different weights (1, 4, and 8 g) were added to a fixed concentration of iron and manganese solution under identical conditions to prepare the product of nano-adsorbent and then reacted with different concentrations of E2 solution ranging from 0.2 to 6 mg/L.

In the adsorption kinetics experiment, the experiment was conducted under E2 solution of 2 mg/L and different contact times to determine the minimum reaction time required to achieve the adsorption equilibrium.

The sorption isotherms and thermodynamic properties were determined by using batch tests; 5 mg adsorbent was added to 250 mL glass conical flasks containing 100 mL E2 solution with concentration ranging from 0.5 to 6 mg/L. Then, the glass conical flaks were shaken for 12 h under different reaction temperatures (298, 308, and 318 K).

To explore the effect of initial solution pH on the adsorption properties, the study was carried out under different pH values (from 3 to 12) with the initial E2 concentration of 2 mg/L. The expected value of solution pH was adjusted by adding 0.1 M HCl or NaOH solution with a negligible volume and measured using pH meters (PHS-3C).

In the experiment of investigating the effect of ionic strength on the adsorption capacity, the expected value of NaCl concentration in E2 solution was adjusted by adding NaCl reagent to 100 mL E2 solution while other conditions remained unchanged.

The common ions in natural water, such as K^+, Na^+, Ca^+, Mg^{2+}, and Cl^-, might interfere with the removal of organic pollutants by forming complexes or occupying active adsorption sites of adsorbents. So, the effect of common electrolyte ions on the adsorption performance was explored. At the same time, the effect of ion valency on adsorption capacity was also considered. The adsorption studies were carried out with 2 mg/L E2 solutions and 5 mg MWCNTs/FMBO under different electrolyte ions.

Elution and regeneration experiments

To evaluate the stability and reusability of adsorbent, the MWCNTs/FMBO which had been used to adsorb E2 was washed repeatedly with 50 mL 4 wt% NaOH solution. The sample particles were transferred into a 100-mL glass conical flask containing 50 mL pure acetone, and the conical flask was stirred at 298 K and 200 rpm for 12 h (Awual 2017b; Jiang et al. 2016). After the elution process, the nanocomposite separated from the solution was rinsed repeatedly with 50 mL deionized water and finally dried at 353 K for reuse in the adsorption cycle.

Results and analysis

Characterization of MWCNTs/FMBO

The N_2 adsorption–desorption isotherm studies demonstrated that the specific surface area of samples with different dosages of stabilizer had obvious difference. According to previous studies, the specific surface area of ferric oxides using the Barrett–Joyner–Halenda (BJH) model was around 6.4–320 m^2/g, mostly depending on the modified method, processing time, and drying means (Cornell and Schwertmann 1997). In the experiments, the powdered adsorbents prepared using 0, 1, 4, and 8 g of stabilizer had specific surface area of 197.6, 147.1, 163.9, and 250.3 m^2/g, respectively, which indicated that the specific surface areas of the target adsorbents were greatly changed by the Fe–Mn oxides loaded on carbon nanotubes. The results of the pore volume and average pore diameter of materials obtained by the BET test are summarized in Table S1. In order to determine the appropriate amount of stabilizer, further adsorption comparison experiments were investigated. The SEM and TEM images of the MWCNT/FMBO nanocomposite are depicted in Fig. 1, which described

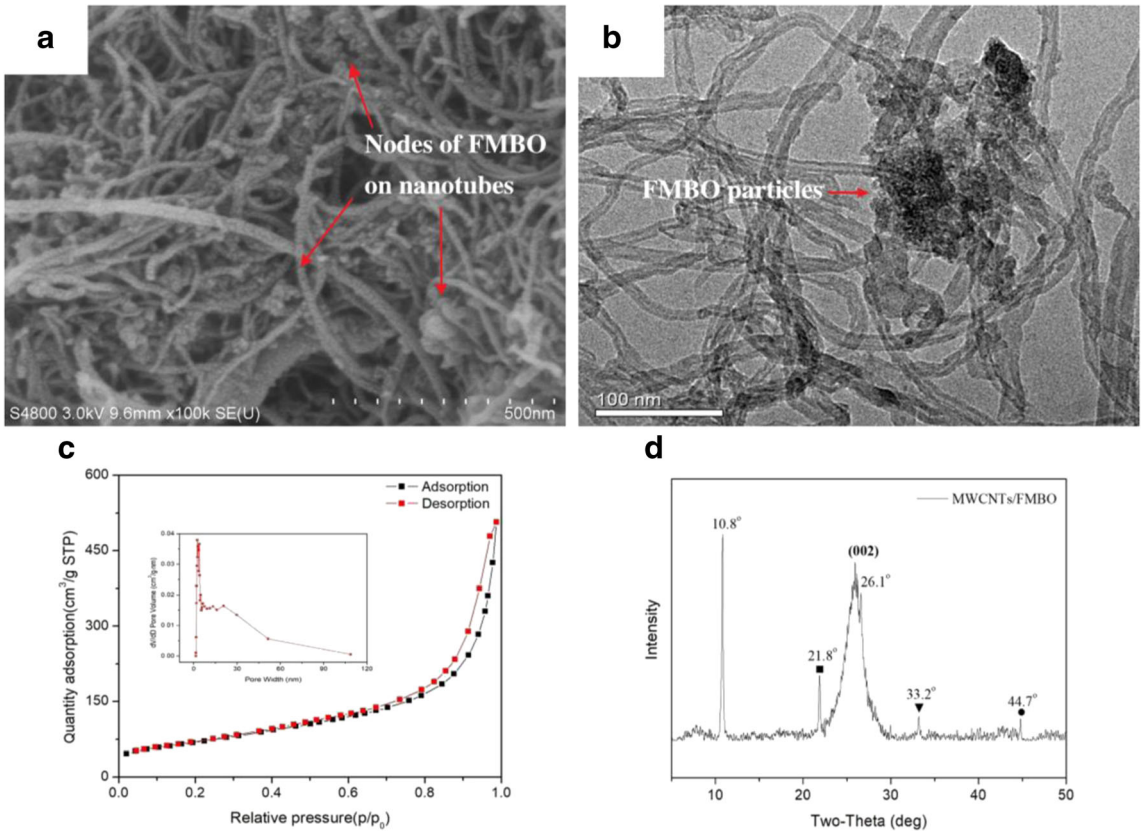

Fig. 1 Characterization of MWCNTs/FMBO: **a** SEM photograph; **b** TEM image; **c** nitrogen adsorption–desorption isotherms (the inset shows the pore size distribution of the sample); **d** XRD pattern (square, MnO_2; inverted triangle, manganese ferrite; circle, Mn_3O_4)

the morphology and microstructure of the sample. As shown in Fig. 1a, the target adsorbent has a much rougher surface and more internal porous structure after the grafting of FMBO nanoparticles onto the surface of MWCNTs. It was revealed by the TEM image of the mesoporous adsorbent in Fig. 1b that many granular nanoscale FMBO particles were successfully grafted onto the surface of MWCNTs and became the points connecting multiple carbon nanotubes, which increased the specific surface area and porosity of the products. In addition, as can be seen from Fig. 1c, the nitrogen adsorption–desorption curve of the materials in the test is shown as H3 hysteresis ring, indicating that the surface of the material is mixed with the micro–mesoporous. Meanwhile, the pore size distribution of the products also confirmed this conclusion. It can be found from the illustration in Fig. 1c that the mesoporous structure occupies an absolute predominance and a small portion of the microporous pores is present on the prepared material surface, which is advantageous for the next series of adsorption experiments.

The XRD pattern of the MWCNTs has been reported earlier. It has two characteristic peaks, $2\theta = 26.1°$ and $2\theta = 43.1°$, respectively (Zhang et al. 2002). As shown in Fig. 1d, the XRD image of the MWCNT/FMBO nanocomposite confirms the presence of a MWCNT phase. The peak at 26.1° corresponds to the reflection of MWCNTs (Zhang et al. 2002), and the peak at 10.8° corresponds to the reflection of a single atomic layer of carbon (Jiang et al. 2016). As revealed by the XRD pattern, according to previous studies (Cui et al. 2014; Li et al. 2017a), the peaks at 21.9° and 33.2° correspond to the reflection of MnO_2 and manganese ferrite, respectively. Meanwhile, the peak at 44.7° matches with the reflection of Mn_3O_4. The analysis results of the XRD pattern indicated that the manganese ferrite nanoparticles were successfully loaded on the surface of CNTs, which was consistent with SEM images.

The hysteresis loop in Fig. S1 for the MWCNTs/FMBO presented an S-shaped curve with on obvious hysteresis curve, indicating that the material had a superparamagnetic property (Kong et al. 2014). The almost zero magnetic coercivity and remanence shown in the illustration also supported this conclusion (Li et al. 2017c). In addition, from Fig. S1, the saturation magnetization of MWCNTs/FMBO was 0.85 emu g^{-1}, suggesting that a small amount of $Fe(NO_3)_3$ was converted into Fe_3O_4 during the synthesis process and caused the weak magnetism property of MWCNT/FMBO nanomaterials.

Effect of stabilizer dosage

The influences of MWCNT concentration on aqueous E2 removal were investigated. In general, the addition of the

stabilizer amount could obviously affect the removal capacity of the adsorbents. As to the optimization of the added amount of stabilizer, the adsorption capacity of the novel adsorbent of MWCNTs/FMBO on E2 was tested at different stabilizer dosage (1, 4, and 8 g MWCNTs). Figure 2 shows the relationship between stabilizer mass and E2 removal effect. It can be found that the adsorbent's adsorption capacity increased steadily with increasing concentration of E2 from 0.2 to 6.0 mg/L. In the concentration range of the experimental work, when the dosage of the stabilizer was 4 g, the E2 adsorption capacity of the sample was better than that of 1 and 8 g. There are two possible reasons for this phenomenon: on the one hand, the small amount of stabilizer made the volume of ferromanganese oxide precipitates loaded on carbon nanotubes to be too large, resulting in decreases of surface area and adsorption capacity of the product, which could be verified by the measurement results of BET. On the other hand, the excess amount of stabilizer made the ferromanganese oxide precipitates loaded on carbon nanotubes insufficient, which led to the limited improvement of adsorption effect.

Kinetics of E2 removal by the MWCNTs/FMBO

The relationship between contact time and E2 removal effect is shown in Fig. 3. As depicted in Fig. 3, nearly 80% of the E2 in the solution was adsorbed within 6 h of the reaction. When the reaction reached equilibrium, the MWNCT/FMBO's adsorption capacity of E2 was 34.72 mg/g. It could be found that the adsorption reaction developed rapidly within the first 10 min, and then reached the adsorption equilibrium within 12 h. Based on the results of the study above, the equilibrium time of adsorption reaction was determined to be 12 h.

To further explore the mechanism of adsorption, three commonly used adsorption kinetic models, namely pseudo-first-order, pseudo-second-order, and intraparticle diffusion, were proposed to interpret the sorption kinetics. Figure 3 shows the simulation results of the models to the experimental data. The equation of intraparticle diffusion model is shown below (Boparai et al. 2011; Zhang et al. 2011):

$$q_e = k_p t^{0.5} + C \quad (2)$$

where k_p is the rate constant of the intraparticle diffusion model (mg/g $min^{1/2}$) and C is a constant related to the thickness of the boundary layer (mg/g).

The kinetic parameters and correlation coefficients calculated based on the experimental data are shown in Table 1. It is found from Table 1 that the pseudo-first-order model has low correlation coefficients ($R^2 = 0.8941$) and the q_e value calculated is quite different with the experimental value. The pseudo-second-order kinetics model is effective in fitting experimental data, which can be demonstrated by the corresponding regression coefficient ($R^2 = 0.9978$). Additionally, the plots of q_t versus $t^{0.5}$ of intraparticle diffusion models are presented in Fig. 3b. As shown in Fig. 3b, it is noticed that the linear plot shows multilinearity in the whole reaction time range, indicating that there are three stages in the adsorption process (Singh et al. 2012). The first stage had a large slope because of the transfer of the target pollutant from the boundary film to the exterior surface of the adsorbents by the film diffusion effect (Zeng et al. 2016). The next stage was the intraparticle diffusion on sorbents, in which the E2 molecules diffused to the inner surface of the adsorbent. The third stage of the reaction reached adsorption saturation, which was caused by the lack of available adsorption sites on the surface. Therefore, the intraparticle diffusion was the rate control stage of the entire sorption process.

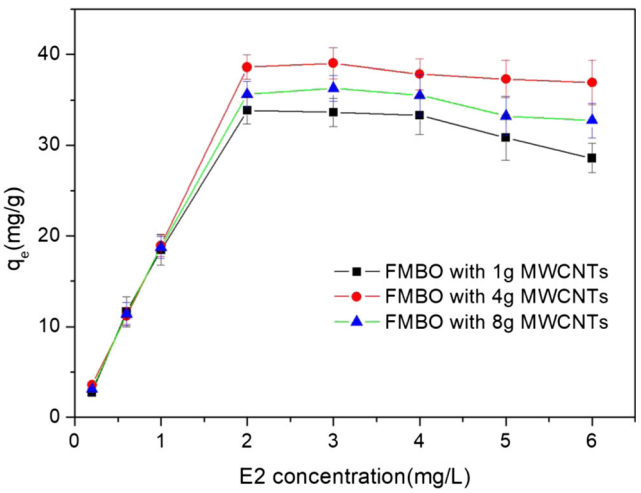

Fig. 2 Effects of stabilizer concentration on removal of E2 by MWCNTs/FMBO nanoparticles (m/V = 0.05 g/L; initial solution pH = 7.0 ± 0.2; t = 12 h; T = 298 K)

Adsorption isotherm of E2 removal by the MWCNTs/FMBO

Figure 4 depicts the absorption effect of MWNCTs/FMBO on E2 at three different temperatures. It is noticed that the increases in adsorption capacity of MWCNTs/FMBO to E2 have a close affinity with the increases in initial E2 concentration at the low initial contaminant concentrations. This is due to the presence of a large number of available adsorption sites on the adsorbent surface. However, as the initial concentration of the pollutant increased continuously, the growth trend gradually slowed down, which indicated that the available adsorption site gradually decreased until the reaction reached equilibrium. The fitting results of the experimental data by the Langmuir and Freundlich models are shown in Table 2. It is found that the Langmuir model outperforms the Freundlich model by comparing the values of correlation coefficient (R^2) and chi-square test (χ^2), suggesting the adsorption of E2 on MWCNTs/FMBO is monolayer adsorption.

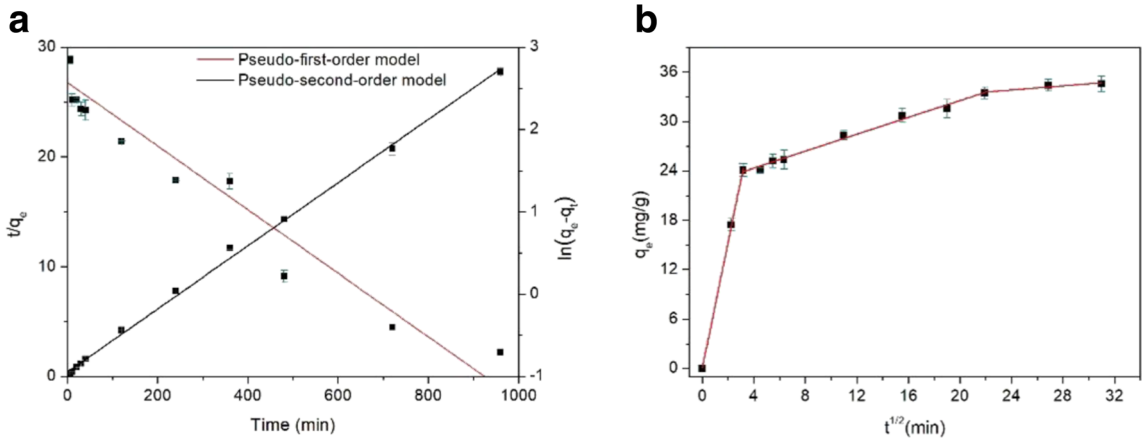

Fig. 3 Kinetics of E2 sorption onto MWCNTs/FMBO: **a** pseudo-first-order and pseudo-second-order sorption kinetics; **b** intraparticle diffusion kinetics (m/V = 0.05 g/L; C_{E2} = 2 mg/L; initial solution pH = 7.0 ± 0.2; t = 12 h; T = 298 K)

In recently published studies, various materials have been explored to purify E2 in water. The theoretical adsorption capacity of SWNTs to E2 was around 26 mg/g (Zaib et al. 2012), while that of MWCNTs was close to 25 mg/g (Sun and Zhou 2014). Besides, the adsorbent of GO also had great potential for adsorbing E2 from aqueous solutions and exhibited a high adsorption capacity, and the adsorption capacities calculated by the Langmuir model were 149.4 mg/g (Jiang et al. 2016). The results of the comparison of the maximum adsorption capacity of E2 between the materials in this work and other adsorbents reported are summarized in Table 3. Compared with the adsorbents above, the adsorbent of MWCNTs/FMBO prepared in this experiment had a preferable performance in E2 adsorption (47.25 mg/g), indicating that MWCNTs/FMBO is a potential adsorbent in removing E2 contaminations.

Table 1 Kinetic parameters for adsorption of E2 on MWCNTs/FMBO

Model	Parameters	Adsorbents
Pseudo-first-order	$q_{e,1}$ (mg/g)	13.09
	k_1 (1/min)	3.86E-03
	R^2	0.8941
Pseudo-second-order	$q_{e,2}$ (mg/g)	34.77
	k_2 (g/mg min)	1.97E-03
	R^2	0.9978
Intraparticle diffusion	$K_{id,1}$	7.66
	C_{i1}	0.08
	R_1^2	0.9993
	$K_{id,2}$	0.51
	C_{i2}	22.30
	R_2^2	0.9886
	$K_{id,3}$	0.12
	C_{i3}	30.86
	R_3^2	0.7758

Adsorption thermodynamic study

The corresponding thermodynamic parameters at 298, 308, and 318 K were determined by the equilibrium constants of the Langmuir model as summarized in Table 4. The negative value of $\triangle H°$ revealed the exothermic nature of adsorption. The values of $\triangle G°$ were negative at three temperatures and became more negative as temperature increased, which suggested that the adsorption reaction was spontaneous. In addition, the positive value of $\triangle S°$ at three temperatures reflected the change in the order of the solid–liquid interphase, which supported the above conclusion.

Effect of solution pH on E2 removal

In general, the solution pH exerted a direct influence on the removal of the target pollution by changing the surface charge

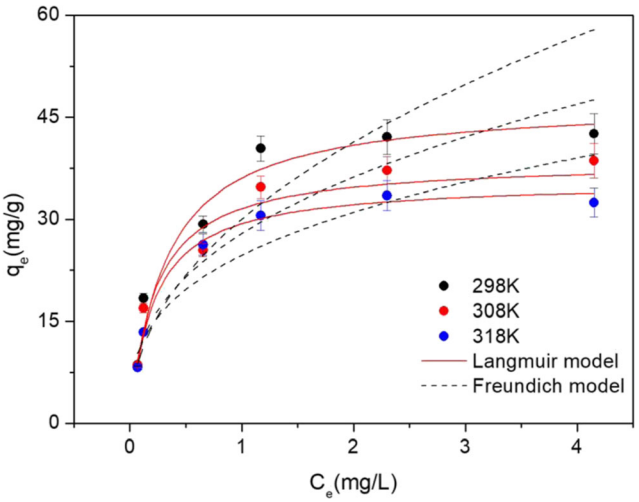

Fig. 4 Effect of initial E2 concentration for the evaluation of maximum adsorption capacity at three different temperatures where the data were fitted on the Langmuir adsorption isotherms model (initial E2 concentration range 0.5–6.0 mg/L; contact time 12 h; m/V = 0.05 g/L; initial solution pH = 7.0 ± 0.2)

Table 2 Langmuir and Freundlich isotherm parameters for adsorption of E2 on MWCNTs/FMBO

T (K)		298	308	318
Langmuir	q_m (mg/g)	47.25	38.48	35.55
	K_L (L/mg)	3.217	4.576	4.730
	R^2	0.973	0.973	0.996
	RMSE	3.752	3.122	0.991
	χ^2	14.078	9.746	0.983
Freundlich	K_f [(mg/g)/(mg/L)^N]	30.04	27.92	24.71
	N	0.461	0.375	0.330
	R^2	0.922	0.941	0.931
	RMSE	6.257	4.592	3.829
	χ^2	39.153	21.089	14.661

distribution of nanometer particle contaminants in solution (Yan et al. 2017). In addition, the solution pH also exerted a significant influence on estrogen oxidation by manganese dioxide, and the pH dependence of organic compound oxidation by manganese oxide has been extensively reported (McArdell et al. 1998; Rubert IV and Pedersen 2006; Zhang and Huang 2003). Figure 5 shows the E2 adsorption efficiency and zeta potential of MWCNTs/FMBO when the adsorption reaction reaches equilibrium at different initial pH values. As illustrated in Fig. 5, it is found that the uptake of E2 by MWCNTs/FMBO highly depends on the initial solution pH. The maximum adsorption capacity of E2 on nanoparticles was 37.7 mg/g when the initial pH was 7.0. However, the adsorption capacity of the nanocomposite decreased sharply above pH 10.0 and reduced to 26 mg/g at pH 12.0. According to its pK_a of 10.4 (Lee et al. 2005), E2 exists mostly in neutral form within the pH range of 3.0–9.0 and deprotonating at pH above 10.0. It can be seen from Fig. 5 that the surface of MWCNTs/FMBO has changed at pH value of 5.5. The nanoparticles of the adsorbent showed a lower adsorption capacity at pH < 5, which could be explained by the FMBO particles loaded on the multiwalled carbon nanotubes that had less solubility in the strong acidic solution and the H^+ in the solution competed with E2 for adsorption activity sites (Jiang et al. 2017). When the pH was around 7.0, the negative charge on the surface of MWCNTs/FMBO was maximized, which was conducive to adsorb E2 molecules because of the electrostatic interaction. The removal rate of E2 was drastically reduced when the pH value was higher than 10, which might due to the decline of the oxidation ability of MnO_2 in an alkaline environment. Moreover, the increase of hydrophilicity on particle surface limited the accessibility of E2 molecules to adsorption sites, which was another reason for the decrease of removal efficiency (Xu et al. 2008).

Table 4 Thermodynamic parameters of E2 adsorption on MWCNTs/FMBO

T (K)	K	$\triangle G°$ (kJ/mol)	$\triangle S°$ (kJ/K mol)	$\triangle H°$ (kJ/mol)
298	7342.2	− 22.05	0.055	− 5.764
308	6445.8	− 22.46		
318	6322.5	− 23.14		

Effect of ionic strength on E2 removal

It is well known that the inorganic ions in natural water are highly reactive toward both metals and surfaces of natural

Table 3 Comparative analysis for the E2 adsorption using different materials

Adsorbents	Basic properties			Quantity adsorbed (mg/g)	Experiment conditions			References
	Specific surface area (m^2/g)	Total pore volume (cm^3/g)	Average pore diameter (nm)		pH	C_0 (mg/L)	Adsorbent amount (mg)	
Biochar (rice straw)	11.13	0.01	5.63	32.41	3.5	6	5	Yin et al. (2019)
Attapulgite	102.42	0.02	2.06	28.12	3.5	6	5	Yin et al. (2019)
Attapulgite/biochar (ATP/BC)	203.38	0.09	1.94	154.23	3.5	6	5	Yin et al. (2019)
Activated carbons	991–1831	0.460–1.149	1.77–3.13	21.3–67.6	5.0	1.0×10^{-3}	10	Tomoko et al. (2006)
Activated magnetic biochar	357.84	0.22	2.25	153.20	5.0	6	5	Yin et al. (2018)
Few layered graphene oxide nanosheets	92	–	2.69	149.40	7.0	3	3	Jiang et al. (2016)
CGMG	298.9	–	–	85.80	7.0	2	5	Jiang et al. (2017)
Hydrochar–FMBO	167.17	0.118	–	49.77	7.0	6	5	Ning et al. (2017)
Single-walled carbon nanotubes	–	–	–	27.20	7.5	–	–	Zaib et al. (2012)
Multiwalled carbon nanotubes	–	0.592	12.14	27.20	–	2.4	5	Sun and Zhou (2014)
MWCNTs/FMBO	163.9	0.474	11.63	47.25	7.0	2	5	This study

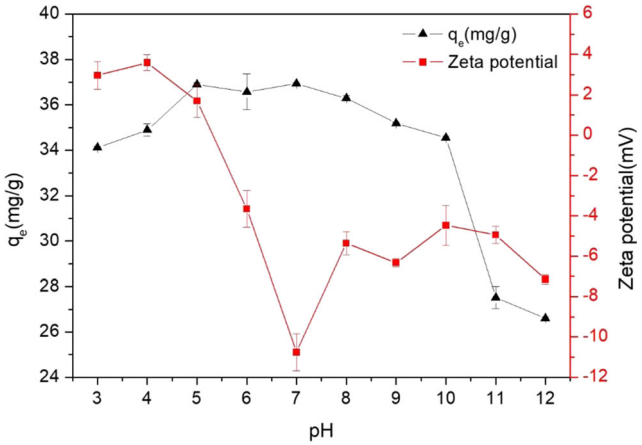

Fig. 5 Effect of the solution pH (m/V = 0.05 g/L; C_{E2} = 2 mg/L; t = 12 h; T = 298 K)

organic matters. Therefore, it might potentially interfere with the removal of target contaminants (Xu et al. 2012). Thus, the interference of ionic strength on the adsorption of E2 by nanoparticles of adsorbent was investigated. As shown in Fig. 6, it is evident that the sorption capacity of E2 by nanoparticles is improved rapidly with the increases of initial NaCl concentration and then reaches the maximum value of 37.78 mg/g when the concentration of NaCl increases to 0.005 M. The reason for this phenomenon is that the enhancement of ionic strength in solution promotes the salting-out effect of hydrophobic organic pollutants, resulting in increases of adsorption capacity of MWCNTs/FMBO (Zhang et al. 2010a). When the NaCl concentration was below 0.005 M, it was obvious that the salting-out effect was enhanced with the increases of ionic strength in solution, which resulted in the rapid increase in E2 adsorption capacity. However, the adsorption capacity of E2 decreased gradually when the concentration of NaCl was

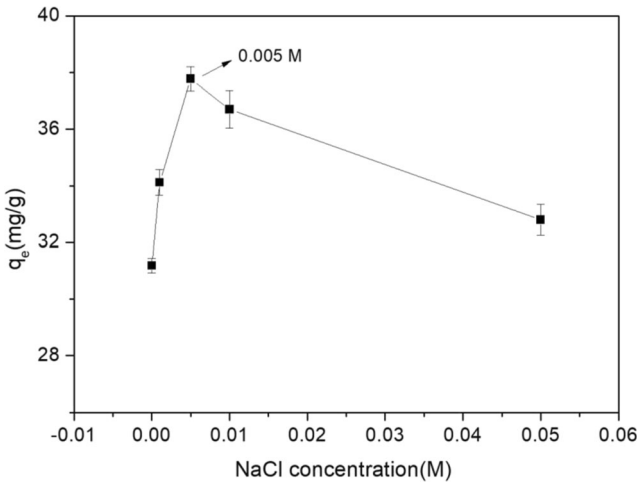

Fig. 6 Effects of the ionic strength on the removal of E2 by MWCNTs/FMBO (m/V = 0.05 g/L; C_{E2} = 2 mg/L; initial solution pH = 7.0 ± 0.2; t = 12 h; T = 298 K)

above 0.005 M, which might due to that the enhancement of squeezing-out effect led to the polymerization of adsorbent particles and resulted in the weakening of adsorption properties (Zhang et al. 2010c).

Effect of background electrolyte on E2 removal

The common ions such as Mg^{2+}, SO_4^{2-}, NO^{3-}, and PO_4^{3-} are usually present in wastewater, which might interfere with the removal of E2 by forming complexes or occupying active adsorption sites of the adsorbent. The effects of background cations such as Na^+, K^+, Mg^{2+}, and Ca^{2+} on the removal process are shown in Fig. 7a. As the most common cations in natural water, Na^+, K^+, Ca^{2+}, and Mg^{2+} had no obvious inhibitory effect on the adsorption process in experimental work. Figure 7b illustrates the effects of background anions such as Cl^-, NO_3^-, SO_4^{2-}, and PO_4^{3-} on the removal process. The experimental results showed that the addition of PO_4^{3-} had a slight inhibition on E2 removal than other anions. It was mainly due to the hydrolysis of PO_4^{3-} that caused the rise of the solution pH and the coordination reaction of PO_4^{3-} with FMBO particles at room temperature, which hardened the surface of the nanomaterials.

Analysis of adsorption mechanism

XPS analysis

XPS is a technique for analyzing the surface chemical properties of materials. It can be used to measure the composition and chemical and electronic states of elements in materials. Figure 8a exhibits the XPS survey spectra of MWCNTs before and after the loading of iron manganese oxides. It was obtained from the XPS spectra where the original samples contained only two elements, carbon and oxygen, which were 96.8 and 3.2%, respectively. The element contents of C, O, Fe, and Mn in the MWCNTs/FMBO were 95.0, 3.9, 0.8, and 0.3%, respectively. The atomic ratio of Fe/Mn in the product was close to 3:1, which was consistent with the amount preparation process.

The XPS spectra of the iron element on adsorbent during the reaction process are shown in Fig. 8b. The peak positions of $Fe2p_{1/2}$ at 724 eV and $Fe2p_{3/2}$ at 711 eV corresponded to FeOOH (Li and Zhang 2007) and had no change after the reaction, suggesting that the iron loaded on the adsorbent was not reduced during the reaction.

Furthermore, Fig. 8c, d compares the XPS spectrum of Mn on adsorbent before and after reaction with E2. It was found that there were two distinct peaks in the XPS spectrum of Mn before E2 processing, and the corresponding components were Mn^{4+} and Mn^{3+}, respectively. The peaks at 654.2 and 643.7 eV were ascribed to Mn^{4+} for MnO_2, and the peak at 642.2 eV was in agreement with the Mn^{3+} for MnOOH (Li

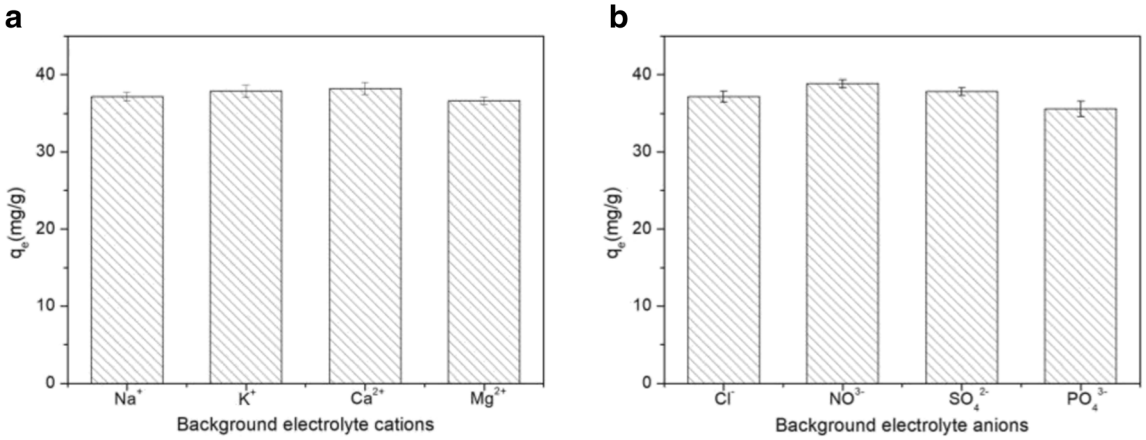

Fig. 7 **a** Effects of background electrolyte cations. **b** Effects of background electrolyte anions (m/V = 0.05 g/L; C_{E2} = 2 mg/L; initial solution pH = 7.0 ± 0.2; t = 12 h; T = 298 K)

et al. 2015; Xu et al. 2015). The result of the fitting curve showed that the content of Mn^{4+} was 68.95% and Mn^{3+} is 31.05%. However, after processing with E2, the peak at 643.7 eV in the spectrum of $Mn2p_{3/2}$ disappeared, indicating decreases in the content of Mn^{4+}. The peak at 641.5 eV in the spectrum of $Mn2p_{3/2}$ implied the emergence of Mn^{2+}. Therefore, the manganese elements on the adsorbent mainly existed in three forms: Mn^{4+}, Mn^{3+}, and Mn^{2+}. By calculating from the fitting curves, the percent of Mn^{4+} was 50.63%, Mn^{3+} was 21.88%, and the percent of Mn^{2+} was 27.49%, suggesting that Mn^{4+} was transformed to Mn^{2+} during the reaction (Jiang et al. 2017). These results suggested that MnO_2 could interact with E2. Therefore, MnO_2 and MnOOH played an important role of oxidation in E2 treatment, and the result was according to previous studies (Jiang et al. 2017; Tang et al. 2016).

In addition, the XPS spectra of O1s in MWCNTs/FMBO before and after the reaction are shown in Fig. 8e, f. Before the reaction with E2, the O1s peaks of MWCNTs/FMBO at 530.22, 531.80, and 533.30 eV were ascribed to O^{2-} from Mn oxide, –OH (hydroxyl bonded to metal), and C–O, respectively (Soria-Sánchez et al. 2011; Toupin et al. 2004). After the reaction, O^{2-} decreased from 26.67 to 18.48%, while C–O increased from 28.30 to 46.16%, which might be assigned to the reduction of Mn^{4+} and the increase in the number of phenolic hydroxyl groups on the surface of the adsorbent after E2 removal (Jiang et al. 2017). Furthermore, the decline in the number of –OH from 45.03 to 35.36% proved the presence of the hydrogen bond between the E2 and the surface of MWCNTs/FMBO.

FTIR analysis

Figure 9a shows the FTIR spectra of the products before and after treatment. It was noticed that from the FTIR spectra, compared to neat MWCNTs, the peak at around 484 cm^{-1} was assigned to the stretching vibration peak of Mn–O, and the peak at 1040 cm^{-1} was attributed to the vibration of –OH in metal hydroxides (Jiang et al. 2017; Liu et al. 2012). After the reaction with E2, it could be found that the aromatic C–H bonds with a peak at around 1450 cm^{-1} and the C=C bonds with a peak at 1650 cm^{-1} increased significantly, which indicated that there was π–π interaction between E2 and MWNCTs/FMBO (Li et al. 2017b). The Mn–O bonds with a peak at 484 cm^{-1} disappeared, illustrating the reduction of manganese oxide (Jiang et al. 2017). In addition, compared with the neat MWCNTs, it was noteworthy that the adsorption peak of the O–H group of MWCNTs/FMBO–E2 complexes shifted from 3420 to 3430 cm^{-1}, testifying that the oxygen-containing functional groups on MWCNTs/FMBO played a crucial role in the adsorption of E2 (An and Zhao 2012).

According to the analysis results of XPS and FTIR spectra, it suggested that there were hydrogen bonds and π–π interaction between the E2 and MWCNTs/FMBO during the adsorption process (Li et al. 2017b). Consequently, the effective adsorption of MWCNTs/FMBO on E2 depended mainly on the hydrophobic structure and hydroxyl group on the surface of nanoparticles. Meanwhile, MnO_2 and MnOOH on the surface of MWCNTs also played an important role during E2 treatment due to its strong oxidation capacity.

Elution and regeneration analysis

Nowadays, both the high adsorption performance for target pollutants and recycling property are the criteria for evaluating the feasibility of materials in practical application (Fan et al. 2011). The data of the adsorption–desorption recycle are summarized in Fig. 9b. As seen, the adsorption capacities of the mesoporous adsorbent remain at 86.16% after five cycles without noticeable loss of capacity, indicating the stability of the MWCNTs/FMBO during the cycles, which would significantly reduce the cost for practical application of the material due to the outstanding regeneration performance.

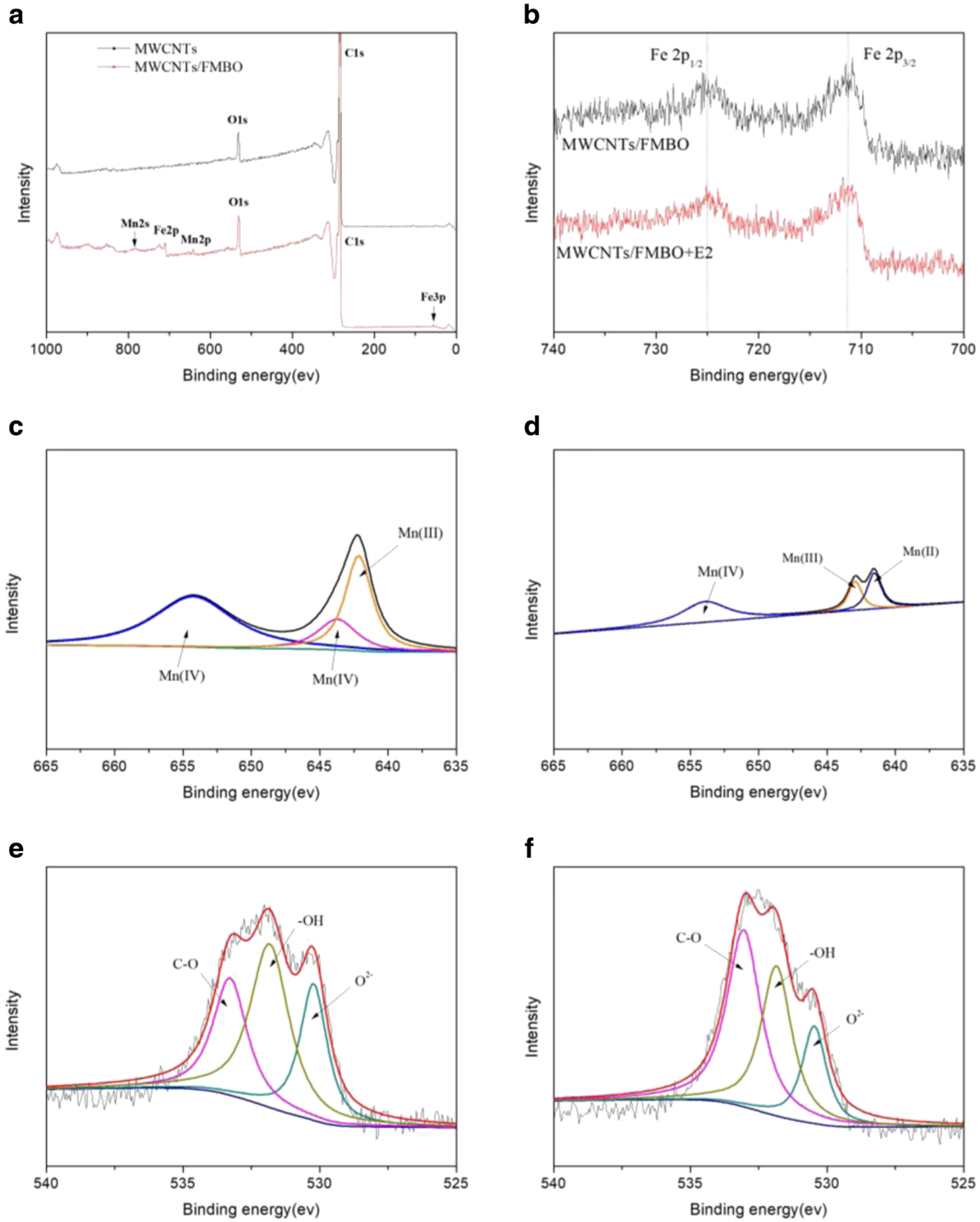

Fig. 8 The high-resolution XPS spectra of MWCNTs/FMBO before and after EE2 removal: **a** full-scan spectra; **b** Fe2p; **c**, **d** Mn2p; **e**, **f** O1s

Conclusions

In this work, MWCNTs/FMBO was successfully synthesized and a range of research results showed that the nanocomposite had an excellent adsorption capacity for E2. Compared with other carbon-based adsorbent reported previously (Sun and Zhou 2014; Zaib et al. 2012), MWCNTs/FMBO had preferable removal effect on E2 under the optimal conditions of 298 K, pH 7.0, and E2 initial concentration of 2 mg/L, and the maximum adsorption capacity (q_m) reached 47.25 mg/g. The experiment data could be well matched by the pseudo-second-order kinetic equation and the Langmuir isotherm model. The thermodynamic studies showed that the adsorption process was exothermic, and the reaction was spontaneous. The reaction process was greatly influenced by the solution pH, especially when pH was more than 10. Besides, the

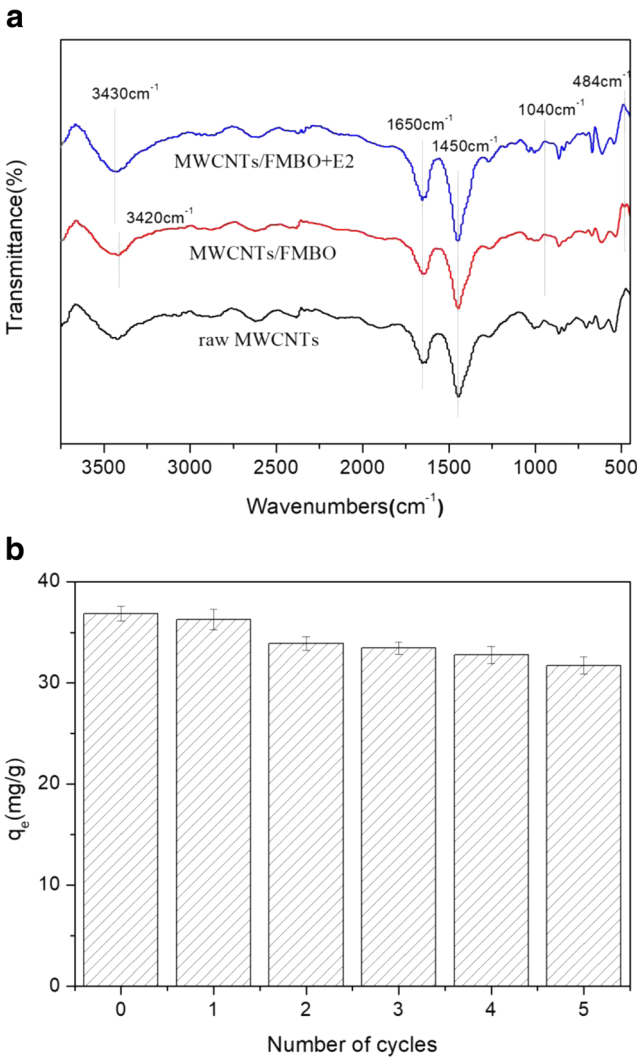

Fig. 9 **a** FTIR spectra of raw MWCNTS and MWCNTs/FMBO before and after E2 adsorption. **b** Regeneration and reuses study of MWCNTs/FMBO (m/V = 0.05 g/L; C_{E2} = 2 mg/L; initial solution pH = 7.0 ± 0.2; t = 12 h; T = 298 K)

changes of ionic strength in the solution had a great influence on the E2 adsorption and the optimal concentration of NaCl was 0.005 M. The common cations such as K^+, Na^+, Mg^{2+}, and Ca^{2+} did not interfere with the adsorption of E2 molecules, but PO_4^{3-} has a slight inhibition on the E2 removal in a certain concentration. In addition, XPS and FTIR analysis showed that adsorption and oxidation occurred simultaneously during E2 removal by MWCNTs/FMBO. The FTIR results also demonstrated that both hydrogen bonds and π–π interaction between MWCNTs/FMBO and E2 might be the dominating mechanism of adsorption. In addition, the nanocomposite has excellent reusability, which is beneficial to reduce the overall cost in wastewater treatment process.

The adsorption mechanism of carbon-based metal oxide nanomaterials on E2 was elucidated in this study, which provided a new idea for environmental pollution control. Aspects of the continuing works should focus on further exploring the adsorption/oxidation mechanism of the removal process by GC/MS analysis and should assess the health threats of by-products through toxicological testing.

Funding information This research was financially supported by the National Natural Science Foundation of China (Grant No. 51609268) and the Key Project of Technological Innovation in the Field of Social Development of Hunan Province, China (Grant Nos. 2016SK2010 and 2016SK2001).

References

An B, Zhao D (2012) Immobilization of As (III) in soil and groundwater using a new class of polysaccharide stabilized Fe–Mn oxide nanoparticles. J Hazard Mater 211:332–341

Awual MR (2017a) New type mesoporous conjugate material for selective optical copper(II) ions monitoring & removal from polluted waters. Chem Eng J 307:85–94

Awual MR (2017b) Novel nanocomposite materials for efficient and selective mercury ions capturing from wastewater. Chem Eng J 307:456–465

Awual MR, Khaleque MA, Ratna Y, Znad H (2015) Simultaneous ultra-trace palladium(II) detection and recovery from wastewater using new class meso-adsorbent. J Ind Eng Chem 21:405–413

Awual MR, Hasan MM, Eldesoky GE, Khaleque MA, Rahman MM, Naushad M (2016) Facile mercury detection and removal from aqueous media involving ligand impregnated conjugate nanomaterials. Chem Eng J 290:243–251

Boparai HK, Joseph M, O'Carroll DM (2011) Kinetics and thermodynamics of cadmium ion removal by adsorption onto nano zerovalent iron particles. J Hazard Mater 186:458–465

Bradley PM, Writer JH (2014) Effect of light on biodegradation of estrone, 17β-estradiol, and 17α-ethinylestradiol in stream sediment. JAWRA J Am Water Resour Assoc 50:334–342

Campbell CG, Borglin SE, Green FB, Grayson A, Wozei E, Stringfellow WT (2006) Biologically directed environmental monitoring, fate, and transport of estrogenic endocrine disrupting compounds in water: a review. Chemosphere 65:1265–1280

Cornell RM, Schwertmann U (1997) The iron oxides: structure, properties, reactions, occurrence and uses. Mineral Mag 61:740–741

Cui HJ, Cai JK, Zhao H, Yuan B, Ai CL, Fu ML (2014) Fabrication of magnetic porous Fe-Mn binary oxide nanowires with superior capability for removal of As(III) from water. J Hazard Mater 279:26–31

Fan Z, Casey FX, Hakk H, Larsen GL (2007) Persistence and fate of 17β-estradiol and testosterone in agricultural soils. Chemosphere 67:886–895

Fan L, Luo C, Lv Z, Lu F, Qiu H (2011) Removal of Ag+ from water environment using a novel magnetic thiourea-chitosan imprinted Ag+. J Hazard Mater 194:193–201

Fan Z, Hu J, An W, Yang M (2013) Detection and occurrence of chlorinated byproducts of bisphenol a, nonylphenol, and estrogens in drinking water of China: comparison to the parent compounds. Environ Sci Technol 47:10841–10850

Huang D-L, Zeng G-M, Feng C-L, Hu S, Jiang X-Y, Tang L, Su F-F, Zhang Y, Zeng W, Liu H-L (2008) Degradation of lead-contaminated lignocellulosic waste by Phanerochaete

chrysosporium and the reduction of lead toxicity. Environ Sci Technol 42:4946–4951

Jiang L-h, Liu Y-g, Zeng G-m, Xiao F-y, Hu X-j, Hu X, Wang H, Li T-t, Zhou L, Tan X-f (2016) Removal of 17β-estradiol by few-layered graphene oxide nanosheets from aqueous solutions: external influence and adsorption mechanism. Chem Eng J 284:93–102

Jiang L, Gu Y, Guo H, Liu L, Chen J (2017) Efficient removal of 17α-ethinylestradiol (EE2) from water using freshly formed Fe–Mn binary oxide. RSC Adv 7:23802–23811

Johnson AC, Dumont E, Williams RJ, Oldenkamp R, Cisowska I, Sumpter JP (2013) Do concentrations of ethinylestradiol, estradiol, and diclofenac in European rivers exceed proposed EU environmental quality standards? Environ Sci Technol 47:12297–12304

Khanal SK, Xie B, Thompson ML, Sung S, Ong S-K, Van Leeuwen J (2006) Fate, transport, and biodegradation of natural estrogens in the environment and engineered systems. Environ Sci Technol 40: 6537–6546

Kong S, Wang Y, Hu Q, Olusegun AK (2014) Magnetic nanoscale Fe–Mn binary oxides loaded zeolite for arsenic removal from synthetic groundwater. Colloids Surf A Physicochem Eng Asp 457:220–227

Lee Y, Yoon J, Von Gunten U (2005) Kinetics of the oxidation of phenols and phenolic endocrine disruptors during water treatment with ferrate (Fe (VI)). Environ Sci Technol 39:8978–8984

Lehman JH, Terrones M, Mansfield E, Hurst KE, Meunier V (2011) Evaluating the characteristics of multiwall carbon nanotubes. Carbon 49:2581–2602

Li XQ, Zhang WX (2007) Sequestration of metal cations with zerovalent iron nanoparticles: a study with high resolution X-ray photoelectron spectroscopy (HR-XPS). J Phys Chem C 111:6939–6946

Li J, Chen J, Yu Y, He C (2015) Fe–Mn–Ce/ceramic powder composite catalyst for highly volatile elemental mercury removal in simulated coal-fired flue gas. J Ind Eng Chem 25:352–358

Li H, Chen Y, Long J, Li X, Jiang D, Zhang P, Qi J, Huang X, Liu J, Xu R (2017a) Removal of thallium from aqueous solutions using Fe-Mn binary oxides. J Hazard Mater 338:296–305

Li MF, Liu YG, Liu SB, Shu D, Zeng GM, Hu XJ, Tan XF, Jiang LH, Yan ZL, Cai XX (2017b) Cu(II)-influenced adsorption of ciprofloxacin from aqueous solutions by magnetic graphene oxide/nitrilotriacetic acid nanocomposite: competition and enhancement mechanisms. Chem Eng J 319:219–228

Li MF, Liu YG, Zeng GM, Liu SB, Hu XJ, Shu D, Jiang LH, Tan XF, Cai XX, Yan ZL (2017c) Tetracycline absorbed onto nitrilotriacetic acid-functionalized magnetic graphene oxide: influencing factors and uptake mechanism. J Colloid Interface Sci 485:269–279

Liu R, Frost RL, Martens WN (2009) Absorption of the selenite anion from aqueous solutions by thermally activated layered double hydroxide. Water Res 43:1323–1329

Liu H, Yang Y, Kang J, Fan M, Qu J (2012) Removal of tetracycline from water by Fe-Mn binary oxide. J Environ Sci (China) 24(2):242–247

McArdell CS, Stone AT, Tian J (1998) Reaction of EDTA and related aminocarboxylate chelating agents with CoIIIOOH (heterogenite) and MnIIIOOH (manganite). Environ Sci Technol 32:2923–2930

Moradi O, Yari M, Zare K, Mirza B, Najafi F (2012) Carbon nanotubes: a review of chemistry principles and reactions. Fullerene Sci Technol 20:138–151

Nakada N, Nyunoya H, Nakamura M, Hara A, Iguchi T, Takada H (2004) Identification of estrogenic compounds in wastewater effluent. Environ Toxicol Chem 23:2807–2815

Ning Q, Liu Y, Liu S, Jiang L, Zeng G, Zeng Z, Wang X, Li J, Kare Z (2017) Fabrication of hydrochar functionalized Fe–Mn binary oxide nanocomposites: characterization and 17β-estradiol removal. Rsc Advances 7: 37122–37129

Petersen EJ, Zhang L, Mattison NT, O'Carroll DM, Whelton AJ, Uddin N, Nguyen T, Huang Q, Henry TB, Holbrook RD (2011) Potential release pathways, environmental fate, and ecological risks of carbon nanotubes. Environ Sci Technol 45:9837–9856

Qin C, Troya D, Shang C, Hildreth S, Helm R, Xia K (2014) Surface catalyzed oxidative oligomerization of 17β-estradiol by Fe3+-saturated montmorillonite. Environ Sci Technol 49:956–964

Rodgers-Gray TP, Jobling S, Kelly C, Morris S, Brighty G, Waldock MJ, Sumpter JP, Tyler CR (2001) Exposure of juvenile roach (Rutilus rutilus) to treated sewage effluent induces dose-dependent and persistent disruption in gonadal duct development. Environ Sci Technol 35:462–470

Rubert KF IV, Pedersen JA (2006) Kinetics of oxytetracycline reaction with a hydrous manganese oxide. Environ Sci Technol 40:7216–7221

Schmitt S, Reifferscheid G, Claus E, Schlüsener M, Buchinger S (2012) Effect directed analysis and mixture effects of estrogenic compounds in a sediment of the river Elbe. Environ Sci Pollut Res 19: 3350–3361

Singh SK, Townsend TG, Mazyck D, Boyer TH (2012) Equilibrium and intra-particle diffusion of stabilized landfill leachate onto micro- and meso-porous activated carbon. Water Res 46:491–499

Soria-Sánchez M, Maroto-Valiente A, Álvarez-Rodríguez J, Muñoz-Andrés V, Rodríguez-Ramos I, Guerrero-Ruíz A (2011) Carbon nanostrutured materials as direct catalysts for phenol oxidation in aqueous phase. Appl Catal B Environ 104:101–109

Sun W, Zhou K (2014) Adsorption of 17β-estradiol by multi-walled carbon nanotubes in natural waters with or without aquatic colloids. Chem Eng J 258:185–193

Szlachta M, Gerda V, Chubar N (2012) Adsorption of arsenite and selenite using an inorganic ion exchanger based on Fe–Mn hydrous oxide. J Colloid Interface Sci 365:213–221

Taguchi T (2016) Encapsulation of cesium from contaminated water with highly selective facial organic-inorganic mesoporous hybrid adsorbent. Chem Eng J 291:128–137

Tang L, Zeng G-M, Shen G-L, Li Y-P, Zhang Y, Huang D-L (2008) Rapid detection of picloram in agricultural field samples using a disposable immunomembrane-based electrochemical sensor. Environ Sci Technol 42:1207–1212

Tang J, Huang Y, Gong Y, Lyu H, Wang Q, Ma J (2016) Preparation of a novel graphene oxide/Fe-Mn composite and its application for aqueous Hg (II) removal. J Hazard Mater 316:151–158

Tomoko F, Satoshi I, Makoto K, Osamu S, Ikuo A (2006) Absorbability of estrone and 17beta-estradiol in water onto activated carbon. Water Research 40: 241–248

Toupin M, Brousse T, Bélanger D (2004) Charge storage mechanism of MnO2 electrode used in aqueous electrochemical capacitor. Chem Mater 16:3184–3190

Wang J, Chen Z, Chen B (2014) Adsorption of polycyclic aromatic hydrocarbons by graphene and graphene oxide nanosheets. Environ Sci Technol 48:4817–4825

Wang F, Sun W, Pan W, Xu N (2015) Adsorption of sulfamethoxazole and 17β-estradiol by carbon nanotubes/$CoFe_2O_4$ composites. Chem Eng J 274:17–29

Wu Z, Zhong H, Yuan X, Wang H, Wang L, Chen X, Zeng G, Wu Y (2014) Adsorptive removal of methylene blue by rhamnolipid-functionalized graphene oxide from wastewater. Water Res 67: 330–344

Xie W, Liang Q, Qian T, Zhao D (2015) Immobilization of selenite in soil and groundwater using stabilized Fe–Mn binary oxide nanoparticles. Water Res 70:485–494

Xu L, Xu C, Zhao M, Qiu Y, Sheng GD (2008) Oxidative removal of aqueous steroid estrogens by manganese oxides. Water Res 42: 5038–5044

Xu J, Wang L, Zhu Y (2012) Decontamination of bisphenol A from aqueous solution by graphene adsorption. Langmuir 28:8418–8425

Xu H, Qu Z, Zhao S, Mei J, Quan F, Yan N (2015) Different crystal-forms of one-dimensional MnO2 nanomaterials for the catalytic oxidation and adsorption of elemental mercury. J Hazard Mater 299:86–93

Yan Z-l, Liu Y-g, Tan X-f, Liu S-b, Zeng G-m, Jiang L-h, Li M-f, Zhou Z, Liu S, Cai X-x (2017) Immobilization of aqueous and sediment-sorbed ciprofloxacin by stabilized Fe-Mn binary oxide nanoparticles: influencing factors and reaction mechanisms. Chem Eng J 314: 612–621

Yin Z, Liu Y, Liu S, Jiang L, Tan X, Zeng G, Li M, Liu S, Tian S, Fang Y (2018) Activated magnetic biochar by one-step synthesis: Enhanced adsorption and coadsorption for 17β-estradiol and copper. Science of the Total Environment 639: 1530

Yin Z, Liu Y, Tan X, Jiang L, Zeng G, Liu S, Tian S, Liu S, Liu N, Li M (2019) Adsorption of 17β-estradiol by a novel attapulgite/biochar nanocomposite: Characteristics and influencing factors. Process Safety and Environmental Protection 121: 155–164

Zaib Q, Khan IA, Saleh NB, Flora JR, Park Y-G, Yoon Y (2012) Removal of bisphenol A and 17β-estradiol by single-walled carbon nanotubes in aqueous solution: adsorption and molecular modeling. Water Air Soil Pollut 223:3281–3293

Zeng W, Liu Y-g, Hu X-j, Liu S-b, Zeng G-m, Zheng B-h, Jiang L-h, Guo F-y, Ding Y, Xu Y (2016) Decontamination of methylene blue from aqueous solution by magnetic chitosan lignosulfonate grafted with graphene oxide: effects of environmental conditions and surfactant. RSC Adv 6:19298–19307

Zhang H, Huang C-H (2003) Oxidative transformation of triclosan and chlorophene by manganese oxides. Environ Sci Technol 37:2421–2430

Zhang H-B, Lin G-D, Zhou Z-H, Dong X, Chen T (2002) Raman spectra of MWCNTs and MWCNT-based H2-adsorbing system. Carbon 40:2429–2436

Zhang S, Shao T, Bekaroglu SSK, Karanfil T (2010a) Adsorption of synthetic organic chemicals by carbon nanotubes: effects of background solution chemistry. Water Res 44:2067–2074

Zhang S, Shao T, Kose HS, Karanfil T (2010b) Adsorption of aromatic compounds by carbonaceous adsorbents: a comparative study on granular activated carbon, activated carbon fiber, and carbon nanotubes. Environ Sci Technol 44:6377–6383

Zhang Y, Ali SF, Dervishi E, Xu Y, Li Z, Casciano D, Biris AS (2010c) Cytotoxicity effects of graphene and single-wall carbon nanotubes in neural phaeochromocytoma-derived PC12 cells. ACS Nano 4: 3181–3186

Zhang C-L, Qiao G-L, Zhao F, Wang Y (2011) Thermodynamic and kinetic parameters of ciprofloxacin adsorption onto modified coal fly ash from aqueous solution. J Mol Liq 163:53–56

Zhang W, Li Y, Wang Q, Wang C, Wang P, Mao K (2013) Performance evaluation and application of surface-molecular-imprinted polymer-modified TiO2 nanotubes for the removal of estrogenic chemicals from secondary effluents. Environ Sci Pollut Res 20:1431–1440